Structures of Active Conformations of UMP Kinase from *Dictyostelium discoideum* Suggest Phosphoryl Transfer Is Associative‡

Ilme Schlichting* and Jochen Reinstein*

Max-Planck-Institut für molekulare Physiologie, Abteilung physikalische Biochemie, Rheinlanddamm 201, D-44139 Dortmund, Germany

Received April 25, 1997; Revised Manuscript Received June 9, 1997⊗

ABSTRACT: UMP/CMP kinase from *Dictyostelium discoideum* ($UmpK_{dicty}$) catalyzes the specific transfer of the terminal phosphate of ATP to UMP or CMP. Crystal structures of $UmpK_{dicty}$ with substrates and the transition state analogs AlF_3 or BeF_2 that lock $UmpK_{dicty}$ in active conformations were solved. The positions of the catalytic Mg^{2+} and the highly conserved lysine of the P loop are virtually invariant in the different structures. In contrast, catalytic arginines move to stabilize charges that develop during this reaction. The location of the arginines indicates formation of negative charges during the reaction at the transferred phosphoryl group, but not at the phosphate bridging oxygen atoms. This is consistent with an associative phosphoryl transfer mechanism but not with a dissociative one.

Phosphoryl transfer reactions are among the most common reactions in biological systems and are catalyzed by ubiquitous enzymes that are generally referred to as kinases, or phosphatases and hydrolases if the acceptor is water. The range of phosphoryl transfer reactions catalyzed by kinases include such important processes as the phosphorylation of enzymes in the control of the cell cyle or metabolism and the activation of nucleosides to nucleotide triphosphates as building blocks of RNA or DNA synthesis. The cascade of kinases that activate nucleosides to nucleoside monophosphates (NMP), then to nucleoside diphosphates, and finally to triphosphates is also of medicinal importance, since it is responsible for the activation of prodrugs such as 3′-azidothymidine (AZT) and (−)-β-L-2′,3′-dideoxy-3′-thiacytidine (3TC) or acyclovir which are among the most potent drugs against HIV or herpes simplex virus, respectively. The reactions catalyzed by NMP kinases are unique since they involve the direct transfer of a phosphate group from one nucleotide to another. Nucleoside diphosphokinases perform the same overall reaction but proceed via a covalent intermediate (ping-pong mechanism), whereas NMP kinases bind both substrates and products simultaneously (bi-bi mechanism). This allowed the design of bisubstrate inhibitors that link the nucleoside triphosphate and the nucleoside monophosphate by an additional phosphate (Lienhard & Secemski, 1973; Feldhaus et al., 1975). These inhibitors have been used widely to investigate the enzymatic mechanism of NMP kinases. We study UMP/CMP kinase from *Dictyostelium discoideum* ($UmpK_{dicty}$)[1] which catalyzes the reversible phosphoryl transfer of ATP to UMP or CMP, giving UDP or CDP in the presence of Mg^{2+}.

Although careful studies have been made on model reactions in free solution (Herschlag & Jencks, 1990), relatively little progress has been made toward understanding the mechanism of enzyme-catalyzed phosphoryl transfer reactions (Knowles, 1980). A controversy has arisen over whether the mechanism is associative or dissociative (Figure 1). Differences in charge formation between these two extremes suggest that catalytic residues of the enzyme should be arranged in distinct ways to stabilize the transition state. Knowledge of the structure of the transition state would allow one to identify the reaction mechanism, but the short lifetime of the transition state renders it inaccessible by direct methods. An alternative approach is to study the binding of compounds that resemble the transition state geometry and charge distribution (Lolis & Petsko, 1990). It has been shown that aluminum fluoride, beryllium fluoride, and vanadate can function as putative transition state analogs for phosphates (Goodno, 1982; Antonny & Chabre, 1992), although it is not obvious why this should be so. Crystal structures of nucleotide complexes of $G_{t\alpha}$, $G_{i\alpha}$, and myosin S1 with aluminum fluoride have been reported (Coleman et al., 1994; Sondek et al., 1994; Fisher et al., 1995). In all these cases, the aluminum was coordinated octahedrally with four equatorial fluoride atoms and two apical ligands, namely oxygen atoms from water and the β-phosphate of GDP or ADP. It is doubtful that this geometry mimics a phosphoryl group as it is being transferred. For the associative mechanism, the transition state is expected to be pentacoordinated with trigonal-planar oxygen atoms. The dissociative mechanism should be structurally similar in the sense that the metaphosphate species would be also planar trigonal, but it should lack coordination to the apical oxygen atoms.

We report here the structure of a complex of an NMP kinase with nucleotides, catalytic Mg^{2+}, and aluminum fluoride. The aluminum fluoride is found to be AlF_3, not AlF_4, and thus formally resembles a transition state of a phosphoryl transfer reaction. The $UmpK_{dicty}$·ADP·CMP·AlF_3·Mg^{2+} structure is compared with the structure without AlF_3 and with a structure with the substrates ADP and UDP

‡ The coordinates were deposited in the Brookhaven Protein Data Bank with the following accession codes: 2ukd for the structure of $UmpK_{dicty}$ with ADP and CMP, 3ukd for the structure with ADP, CMP, and AlF_3, and 4ukd for the structure with ADP, UDP, and BeF_2.

* Authors to whom correspondence should be addressed. Phone: (49)-(231)-1206 366. Fax: (49)-(231)-1206 229.

⊗ Abstract published in *Advance ACS Abstracts,* July 1, 1997.

[1] Abbreviations: $UmpK_{dicty}$, UMP/CMP kinase from *Dictyostelium discoideum* (EC 2.7.4.14); UP_5A, P^1-(adenosine 5′)-P^5-(uridine 5′)-pentaphosphate.

S0006-2960(97)00974-4 CCC: $14.00

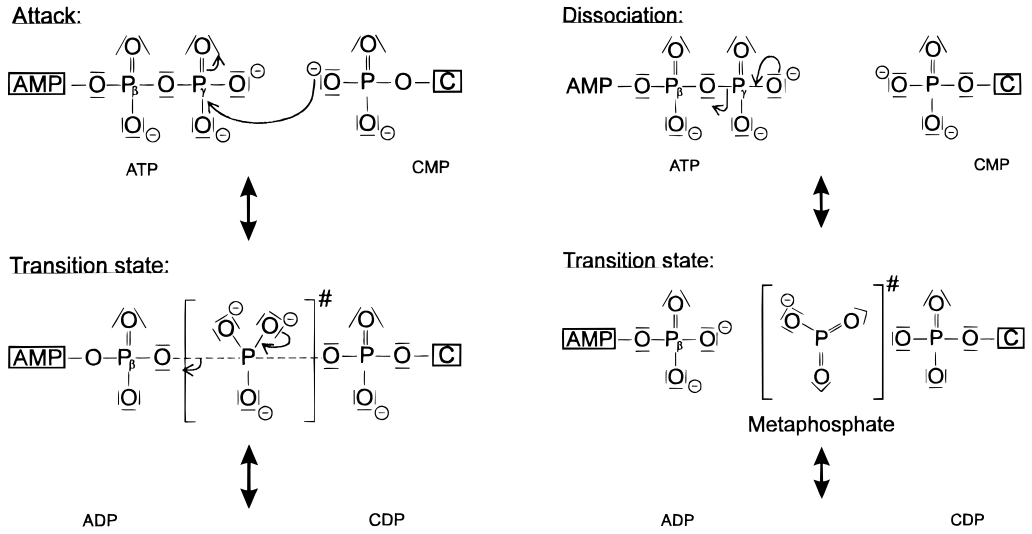

FIGURE 1: Associative *versus* dissociative mechanism of phosphoryl transfer. (A, left) In the associative mechanism of phosphoryl transfer, the bond between the incoming nucleophile (an oxygen atom from CMP here) and the attacked phosphorus atom (P from ATP here) forms before the old bond between P_β and P_γ of ATP is broken. The transition state is pentacoordinated and accumulates three negative charges at the transferred phosphoryl group. The formation of charge for the forward reaction (ATP + CMP) and backward reaction (ADP + CDP) is the same. (B, right) In the dissociative mechanism (right), the P_β and P_γ bond of ATP is broken before the new bond is formed. The transition state contains the highly reactive intermediate metaphosphate, which is subsequently captured by the acceptor group (CMP here). As is indicated by the arrows, charge accumulates at the $P_\beta-P_\gamma$ bridging oxygen and the transferred phosphoryl group contains one negative charge. The reverse reaction accumulates charge at the bridging oxygen of P_α and P_β of CDP; in this respect, the dissociative mechanism is asymmetric in charge development.

stabilized by beryllium. These structures are used to draw conclusions about the mechanism of phosphoryl transfer reactions.

MATERIALS AND METHODS

Crystallization. $UmpK_{dicty}$ was expressed, purified, and crystallized essentially as described previously (Wiesmüller et al., 1995). Crystals were grown from a solution of 0.64 mM $UmpK_{dicty}$, 0.8 mM ADP, 0.8 mM CMP or UMP, 100 mM Tris/HCl (pH 8.5), 30 mM $MgCl_2$, and 40 mM DTE in the presence or absence of 0.8 mM $AlCl_3$ or $BeCl_2$ and 4 mM NaF using PEG 4000 as a precipitant. The diffraction data were reduced with DENZO (Otwinowski, 1992) or XDS (Kabsch, 1993). The structure of $UmpK_{dicty}$ complexed with UP_5A (Scheffzek et al., 1996) was used as a starting model for refinement with X-PLOR 3.851 (Brünger, 1992) omitting the nucleotide, Mg^{2+}, and water molecules. After several rounds of interactive model fitting with O (Jones et al., 1991) (placing water molecules, the nucleotides, and Mg^{2+}) and refinement (including bulk solvent correction, simulated annealing, and isotropic *B*-factor refinement), the density of AlF_x and BeF_x was fitted. The density for AlF_x is planar and accommodates only three fluorides; thus, we identify it as AlF_3. Although the BeF complex crystals were set up with CMP or UMP, there was strong electron density at the position of the β-phosphate of CMP or UMP. This is consistent with analysis by mass spectroscopy of dissolved crystals that showed the presence of CDP. We surmise that due to the high enzyme concentration in the crystallization setup and the long time it takes to grow the crystals (days) the kinase-catalyzed reactions 2ADP → ATP + AMP and subsequently ATP + CMP → CDP + ADP take place. Beryllium stabilizes the $UmpK_{dicty}$·ADP·CDP complex since it bridges the two β-phosphates and energetically favors this state. Because the crystals containing BeF_x and CDP were setup with equal volumes of ADP and CMP, resulting in about 50% CDP, we set up crystals with a 3-fold excess of ADP over UMP, expecting full occupancy of UDP, which was indeed observed (see Figure 2). We chose UMP instead of CMP to verify at the same time that the base of the mononucleotide has no influence on the features observed in the phosphate region.

Kinetic Studies. Inhibition studies were performed at 25 °C with a coupled colorimetric assay as described (Brune et al., 1985). Experimental conditions were 250 μM ADP, 500 μM CDP, and the inhibitors AlF_x, BeF_x, VO_x, or NO_3^- (each at 0−400 μM) in 100 mM Tris/HCl (pH 7.5), 20 mM DTE, 0.5 mM $NADP^+$, 10 mM glucose, 50 mM KCl, and 5 mM $MgCl_2$. AlF_x and BeF_x were prepared by mixing 1 equiv of $MeCl_x$ with 100 parts of NaF prior to the experiment. The potential inhibitor vanadate was prepared as described (Goodno, 1982).

Stopped flow measurements were performed at 25 °C essentially as described (Theyssen et al., 1996). The buffer for $UmpK_{dicty}$ was 50 mM Tris/HCl (pH 7.5), 20 mM DTE, 100 mM KCl, and 1.6 mM $MgCl_2$. The intrinsic tryptophan signal was monitored at an excitation of 295 nm and a cutoff filter of 345 nm, typically with 50 μM CMP, 250 μM ADP, and 1 μM $UmpK_{dicty}$ in one mixing chamber and 0−500 μM AlF_x or BeF_x in the other syringe. For measurements with the fluorescently labeled bisubstrate inhibitor α,ω-[bis-3′-(2′)-*O*-(*N*-methylanthraniloyl)adenosine-5′-*O*)]pentaphosphate (mAP_5Am) (Reinstein et al., 1990a,b), one syringe typically contained 50 μM CMP, 250 μM ADP, and 0.5 μM $UmpK_{dicty}$, with 0−500 μM AlF_x or BeF_x and 1 μM mAP_5-Am in the other. Excitation was at 360 nm, and emmission was recorded with a cutoff filter at 455 nm.

RESULTS

Kinetic Properties. We screened for possible candidates of transition state analogs by measuring the inhibition of the activity of UMP kinase under steady state conditions with 0-400 μM inhibitor (see Materials and Methods). The maximum inhibition at 250 μM ADP and 500 μM CDP by

Table 1: Data Collection and Reduction Statistics

	no transition state analog	AlF_x transition state analog	BeF_x transition state analog	BeF_x transition state analog
data collection (4 °C)	DESY, BW7B	NSLS, X12-C	NSLS, X12-C	rotating anode
wavelength (Å)	0.83	1.0	1.0	1.54
detector	MAR	MAR	MAR	SIEMENS
data reduction	DENZO	DENZO	DENZO	XDS
data scaling	SCALEPACK	SCALEPACK	SCALEPACK	XSCALE
data collection statistics				
space group $P4_12_12$, unit cell (Å)	$a = b = 78.7$, $c = 100.1$	$a = b = 78.8$, $c = 100.7$	$a = b = 78.5$, $c = 101.3$	$a = b = 78.1$, $c = 101.9$
number of crystals	2	2	2	7
resolution (Å)	2.2	1.9	1.65	2.0
observed reflections	53 982	101 015	219 971	136 023
unique reflections	15 558	24 834	38 069	18 420
completeness (%, overall/last shell)	94/95 (2.32 −2.2Å)	93/79 (1.97−1.90 Å)	90/80 (1.72−1.65Å)	95/81 (2.1−2.0 Å)
R_{merge}[a] (%, overall/last shell)	7.4/22.1	8.7/34.6	6.1/30.3	8.4/36.6

[a] $R_{merge} = |I - \langle I \rangle|/I$.

Table 2: Statistics of Structure Refinement

	no transition state analog	AlF_x transition state analog	BeF_x transition state analog	BeF_x transition state analog
resolution (Å)	37−2.2	9.9−1.9	10−1.65	39−2.0
no. of waters	133	154	151	107
nucleotides	ADP, CMP	ADP, CMP	ADP, CMP/CDP[b]	ADP, UDP[c]
metals	Mg^{2+}	Mg^{2+}, AlF_3	Mg^{2+}, BeF_2	Mg^{2+}, BeF_2
R_{factor}[a]/R_{free} (%)	19.3/23.1	19.8/23.2	21.5/24.1	19.4/21.2
rms deviations				
bond lengths (Å)	0.011	0.011	0.014	0.015
bond angles (deg)	1.19	1.19	1.20	1.24
dihedral angles (deg)	24.3	24.2	25.0	26.2
improper angles(deg)	1.96	2.21	2.04	2.07
average B (Å^2)				
main chain	25.6	25.0	21.8	26.8
side chain	27.3	27.2	23.6	28.4

[a] $R_{factor} = ||F_{obs}| - |F_{calc}||/|F_{obs}|$ (5% randomly omitted reflections were used for R_{free}). [b] Crystals were grown with equal concentrations of ADP and CMP, resulting in ca. 50% CDP. [c] Crystals were grown with a 3-fold excess of ADP over UMP, resulting in a fully occupied β-phosphate of UDP (see Materials and Methods).

AlF_x was 7-fold and by BeF_x 500-fold. Addition of vanadate or nitrate did not cause any observable inhibition. To obtain more detailed data on the dynamics of binding, we measured the transient kinetics of assembly and disassembly of the $UmpK_{dicty}$ transition state analog complexes (see Materials and Methods). The intrinsic tryptophan fluorescence of $UmpK_{dicty}$ decreases upon addition of AlF_x or BeF_x to $UmpK_{dicty}$−nucleotide complexes and thus serves as a signal for binding (data not shown). The formation and disassembly rate coefficients of the transition state analog complexes are very low for AlF_x ($k_{on} = 4 \times 10^3$ M^{-1} s^{-1}, $k_{off} = 0.1$ s^{-1}, and $K_d = 25$ μM) and even lower for BeF_x ($k_{on} = 10^3$ M^{-1} s^{-1}, $k_{off} = 0.005$ s^{-1}, and $K_d = 5$ μM). Dissociation of $UmpK_{dicty}$−nucleotide complexes occurs in the absence of AlF_x or BeF_x with rate coefficients of greater than 1000 s^{-1}. The results obtained by tryptophan fluorescence were confirmed with the fluorescently labeled bisubstrate inhibitor α,ω-[bis-3′(2′)-*O*-(*N*-methylanthraniloyl)-adenosine-5′-*O*-)]pentaphosphate (mAP_5Am). In a stopped flow apparatus, $UmpK_{dicty}$ was incubated with ADP, CMP, and various amounts of AlF_x or BeF_x and rapidly mixed with mAP_5Am (see Materials and Methods). In the absence of nucleotides, mAP_5Am (0.5 μM) binds with a rate of 70 s^{-1}, in the presence of 50 μM ADP and 125 μM CMP with a rate of 26 s^{-1} (data not shown). The presence of 25 μM AlF_x generates a slow phase of binding with a rate of 0.1 s^{-1}, consistent with the release of the transition state analog complex being the rate-limiting step for mAP_5Am binding. The dependence of the amplitude of the fast phase of mAP_5Am binding which decreases upon increasing concentrations of AlF_x or BeF_x indicates how much transition state analog complex was formed prior to the addition of mAP_5Am. This allowed measurement of the affinities of AlF_3 and BeF_2 directly.

Description of Structure. $UmpK_{dicty}$ was cocrystallized with Mg^{2+}, ADP, and CMP or UMP in the presence or absence of AlF_x or BeF_x. The statistics of X-ray data collection are summarized in Table 1, and the refinement statistics are summarized in Table 2. The structures were solved by difference Fourier techniques using the structure of $UmpK_{dicty}$ complexed with the bisubstrate inhibitor P^1-(adenosine 5′)-P^5-(uridine 5′)-pentaphosphate (UP_5A) (Scheffzek et al., 1996) as a starting model. The electron densities of the phosphate regions are shown in Figure 2. The $UmpK_{dicty}$·ADP·CMP complex shows octahedral coordination of the Mg^{2+} ion with five water molecules and the β-phosphate of ADP (Figure 2a). The complex grown in the presence of aluminum fluoride shows a planar AlF_3 centrally located between ADP and CMP (Figure 2b). The 2.0 and 2.2 Å distances of Al^{3+} to the terminal O3B atoms of ADP and CMP, respectively, are likely the same given the estimated mean coordinate error of 0.2 Å. Fluoride F3 occupies roughly the same position as Wat-900 in the structure containing only ADP and CMP, and it also coordinates the Mg^{2+} ion. However, the octahedral coordination of Mg^{2+} is slightly distorted. Fluoride F1 is located

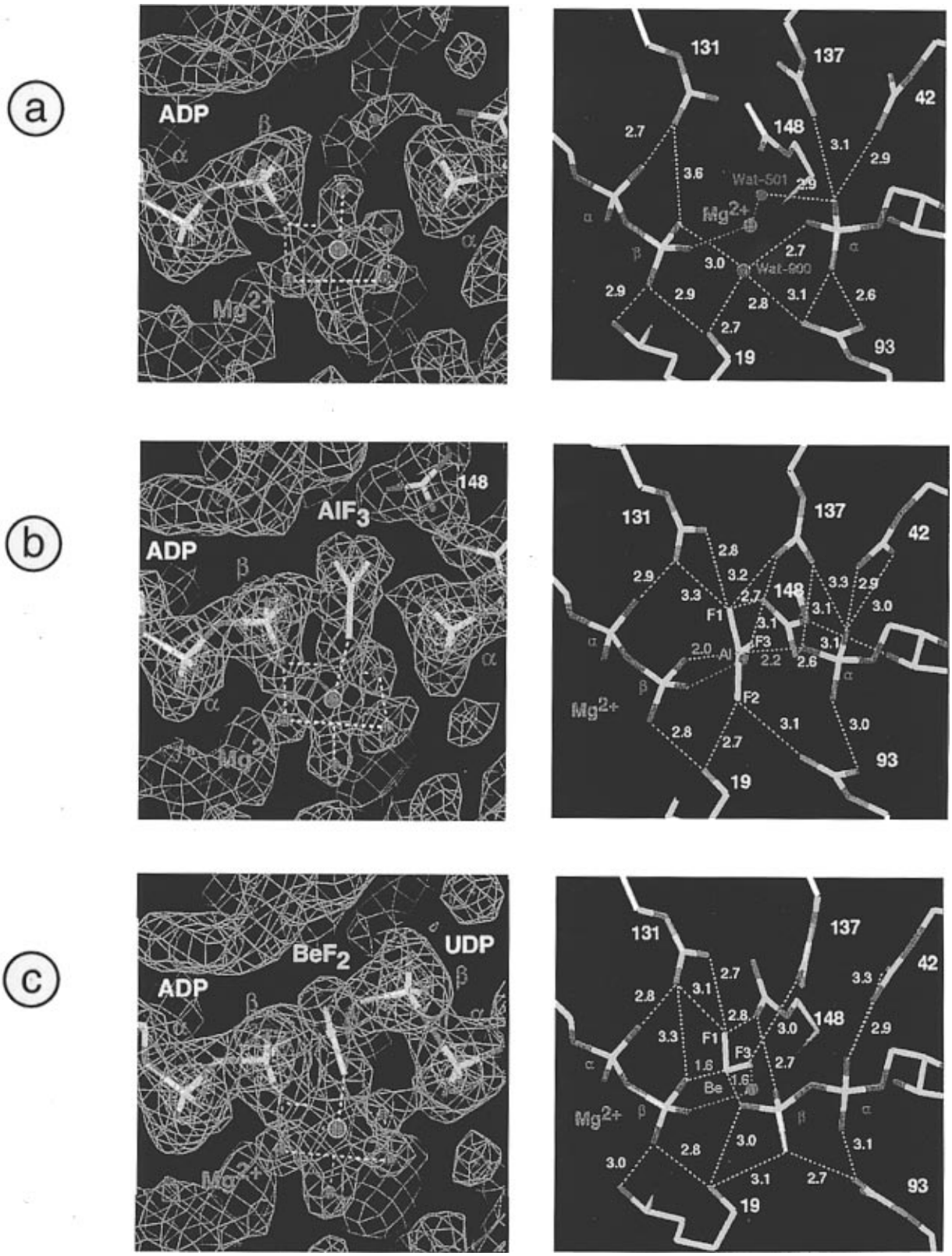

FIGURE 2: Active sites of $UmpK_{dicty}$ complexed with Mg^{2+} and (a) ADP and CMP, (b) ADP, CMP, and AlF_3, and (c) ADP, UDP, and BeF_2. The $3F_{obs} - 2F_{calc}$ electron density maps [cutoff of 1.6σ (cyan) and 6.2σ (magenta)] are shown on the left side, showing the phosphates, the Mg^{2+} (magenta sphere) coordination, AlF_3, and BeF_2 (yellow). The distances to surrounding arginines are shown on the right panel.

close to Wat-501 of the $UmpK_{dicty}$·ADP·CMP complex. Unexpectedly, crystals grown in the presence of ADP, beryllium fluoride, and either CMP or UMP show high electron density for CDP or UDP (see Materials and Methods). In this case, the octahedron around the Mg^{2+} ion is not distorted. The beryllium (which cannot be located by means of the electron density due to its few electrons) was placed in a tetrahedral coordination between the β-phosphates of ADP and CDP or UDP and two fluoride atoms that occupy similar locations as F1 and F3 of the AlF_3 molecule (Figure 2c). Beryllium stabilizes the two nucleotide diphosphates by forming a strong bridge between the terminal O3B oxygen

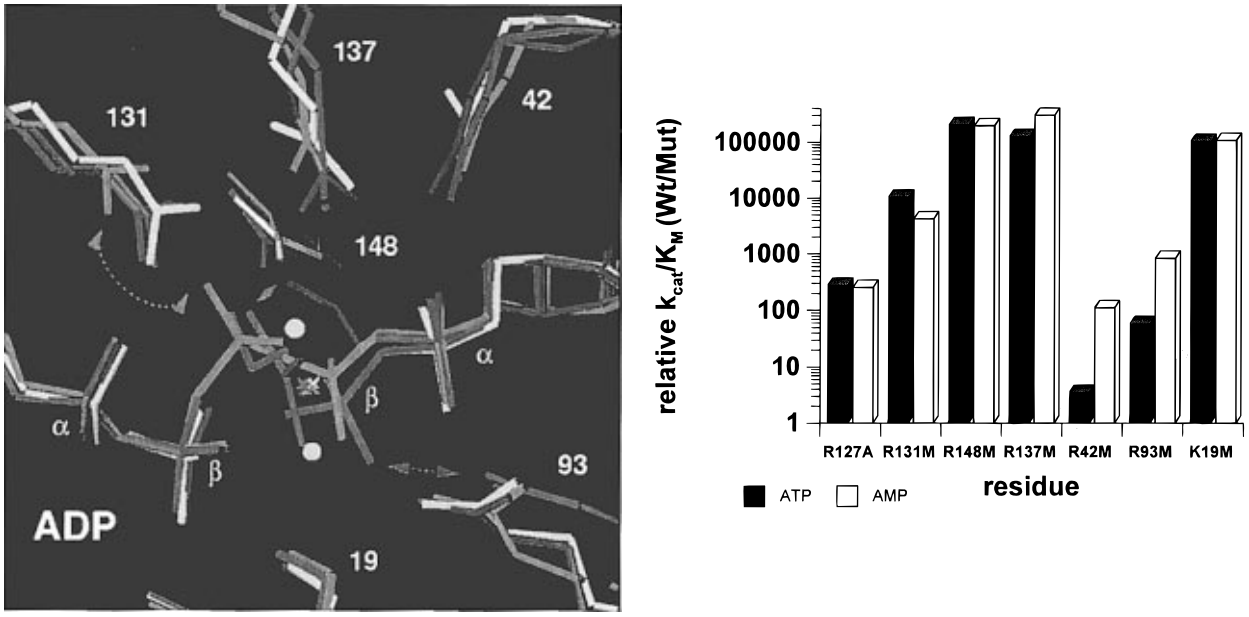

FIGURE 3: (A, left) Overlay of the active sites of $UmpK_{dicty}$ complexed with ADP and CMP (yellow), in the presence of AlF_3 (cyan) or BeF_2 (green), and with UP_5A (magenta) (Scheffzek et al., 1996). The magnesium ions are shown as crosses and water molecules as yellow spheres. The magenta arrow points to the steric hindrance between the bridging phosphate of UP_5A and R131 which prevents complete closing of the LID domain (residues 129−143). The blue arrow indicates that R148 rotates to interact with AlF_3. The green arrow highlights the sterically induced movement of R93 upon the presence of the β-phosphate at the mononucleotide binding site. The position of R137 differs in all structures. It moves in a corkscrew-like fashion toward the fluoride F1 of AlF_3. Neither Mg^{2+} nor K19 moves within the coordinate error of the structures. (B, right) The residues shown in part A are highly conserved in NMP kinases. The effect of mutations of the corresponding residues (Yan et al., 1990a,b; Dahnke et al., 1992) in adenylate kinase from chicken as determined by Tsai and co-workers (numbering according to $UmpK_{dicty}$) is shown. Arginines 131, 137, and 148 from the LID domain and lysine 19 from the P loop have the most dramatic effects on the catalytic efficiency (k_{cat}/K_M).

atoms of ADP and UDP, respectively (see Table 2). Beryllium tends to form polymers to increase its coordination number to 4 (with tetrahedal geometry). A coordination number of 5 (with trigonal bipyramidal geometry) comparable to that of ADP·AlF_3·CMP is not attainable (Bell, 1972). The distances from the nucleotide phosphates, AlF_3, and BeF_2 to the surrounding arginines (42, 93, 131, 137, and 148) are indicated in the right panel of Figure 2. An obvious difference among these complexes is that the arginines in the complex containing only ADP and CMP have very poor electron density, indicating high mobility. The major difference in the location of the arginines is that R148 rotates toward AlF_3 whereas R93 moves due to steric interference when a β-phosphate is present at the mononucleotide binding site to interact with the β-phosphate. Figure 3 shows an overlay of all three structures with the structure of $UmpK_{dicty}$ complexed with the bisubstrate inhibitor UP_5A (Scheffzek et al., 1996). The phosphates of ADP and CMP or UMP are at the same position as the corresponding phosphates in UP_5A, whereas the β-phosphate of UDP occupies a different position. The additional phosphate of UP_5A is close to R131 which therefore moves outward compared to the other structures. This results in a rigid body rotation of the whole LID region (residues 129−143) by 13°. This incomplete closing of the LID in the UP_5A complex is also reflected in the protein main chain temperature factors. While the mobility of most of the protein main chain and the average *B*-factors are comparable in all structures (Table 2), they differ dramatically for the catalytic LID domain. The mobility with the bisubstrate inhibitor UP_5A (Scheffzek et al., 1996) is the highest (mean *B*-factor of 46 Å^2) followed by the complex with ADP·CMP (mean *B*-factor of 38 Å^2). The addition of the transition state analog AlF_3 (mean B-factor of 26 Å^2) or the bridging BeF_2 (mean *B*-factor of 25 Å^2) apparently locks this catalytic region in the catalytically competent conformation of $UmpK_{dicty}$.

DISCUSSION

Why Is the Affinity for AlF_3 So Low? It is surprising that the affinity of AlF_3 for the $UmpK_{dicty}$·ADP·CMP complex is relatively low ($K_d = 25\ \mu M$), although AlF_3 appears to be so precisely fixed in the active site. However, the nucleotide AlF_3 complex is not a covalent transition state analog, so there is an unfavorable entropic factor. Furthermore, the dominant complex formed by $AlCl_3$, NaF, and nucleotide diphosphate in solution appears to be nucleotide diphosphate·AlF_4-OH at neutral pH (Martin, 1996), so the active site of $UmpK_{dicty}$ binds a species that is minor in free solution. This point also relates to the structures of $G_{t\alpha}$ and $G_{i\alpha}$ (Coleman et al., 1994; Sondek et al., 1994) which contain AlF_4-OH probably because the active sites of these rather poor catalysts are too weak to enforce the binding of AlF_3. During the revision of the manuscript, the structure of the efficient enzyme NDP kinase from *D. discoideum* complexed with ADP and AlF_3 was published (Xu et al., 1997). It is thus conceivable that only very efficient enzymes with a snug fit of the transition state (Jencks, 1975) possess perfectly tailored active sites for accommodation of the trigonal phosphate group being transferred, thus preventing binding of the octahedral nucleotide diphosphate·AlF_4-OH complex as it occurs in solution.

Mechanism of Phosphoryl Transfer. In the case of phosphoryl transfer reactions, the enzymatic mechanism may be deduced from the transition state structure. It differs both in charge distribution and bond lengths for the extremes of pure associative and dissociative mechanisms (see Figure 1). The observed distances of 2 and 2.2 Å between Al^{3+} and

the phosphate oxygen atoms are longer than a covalent bond (ca. 1.7 Å) but significantly shorter than the van der Waals distance of roughly 3.5 Å. This indicates substantial bond formation between the transferred phosphoryl group to donor and acceptor nucleotides, which supports an associative mechanism (but does not completely exclude a dissociative mechanism).

For a dissociative mechanism, however, the charge formation during the backward reaction (transfer of the β-phosphate of the nucleotide diphosphate to ADP) would differ from that during the forward reaction (see Figure 1). In this case, one would expect to find a positive residue next to the bridging oxygen between the α- and β-phosphate of UDP in the structure of the beryllium-stabilized $UmpK_{dicty}$·ADP·UDP complex (reaction of ADP with UDP). As can be seen in Figure 2c, no such interaction is observed. Although the positioning of R93 next to the terminal oxygen of the α-phosphate of CMP (which was the bridging oxygen of CDP before the reaction) in the AlF_3 structure would be consistent with a dissociative mechanism (Maegley et al., 1996), this interaction may also be necessary for an associative mechanism. The hydrogen bond renders the attacked phosphoryl group more positively polarized, thereby facilitating a nucleophilic attack by ADP. In this respect, R93 would have a function similar to that of Mg^{2+} at the ADP site for the reverse reaction.

The location of the charges developing during the phosphoryl transfer reaction may be inferred from the position of stabilizing positively charged groups provided by the enzyme. The most conclusive information comes from interactions of the enzyme with AlF_3. In close proximity to AlF_3 are several arginine residues, Mg^{2+}, and the highly conserved lysine (K19) of the P loop (Saraste et al., 1991). Mg^{2+} and K19 [whose mutation results in reduction of the catalytic efficiency by about 5 orders of magnitude (Reinstein et al., 1990a,b; Byeon et al., 1995)] interact with the β-phosphate oxygen atoms of ADP and with the fluorides of AlF_3. The positions of Mg^{2+} and K19 are virtually invariant in the different $UmpK_{dicty}$ complexes (Figure 3A). Our structures suggest that Mg^{2+} with the associated water molecules and K19 provide a template for the phosphoryl transfer reaction. In contrast, the arginine residues indicate where negative charge develops relative to the ground state. As shown in Figure 3A, R137 and R148 rearrange to interact with AlF_3 which mimics the transferred phosphoryl group, indicating that most of the charge compensation takes place here (Warshel & Aqvist, 1991) and not on the phosphate bridging oxygen atoms. The importance of these interactions for stabilization of the transition state is reflected in mutational data (Yan et al., 1990a,b; Dahnke et al., 1992) that show an approximately 10^4-fold decrease of the catalytic efficiency when R131 is replaced by methionine and a 10^5-fold decrease of the catalytic efficiency when R137 or R148 is replaced by methionine (Figure 3B). Interestingly, these three arginine residues belong to the LID domain and undergo the most pronounced structural rearrangements as indicated in Figure 3A. Mutation of the other arginine residues in the active site shows only moderate effects. The extreme density of positive charges that is precisely located around AlF_3 indicates that the transferred phosphoryl group is highly negatively charged, as would be expected for an associative mechanism of phosphoryl transfer. It would strongly disfavor the reaction with a dissociative mechanism since here charge of the transferred group decreases relative to the ground state. We conclude that the mechanism has a strong associative character; bond length and features of bridging oxygen atoms are consistent with it, and the positive charges around the transferred group demand it.

General Implications. The structures of $UmpK_{dicty}$ described here provide snapshots of an enzyme-catalyzed phosphoryl transfer reaction. They indicate that the catalytic machinery of the enzyme (re)assembles before and after catalysis, show that AlF_3 is a transition state analog, and provide firm evidence for an associative mechanism of phosphoryl transfer by NMP kinases. Knowledge of the geometry and charge features of the transition state of NMP kinases is also of practical interest since it provides a blueprint for the design of transition state inhibitors and may be used as a starting point for the generation of inhibitors of medically important kinases such as thymidylate kinase.

ACKNOWLEDGMENT

We thank Petra Herde and Georg Holtermann for skilled technical assistance and Roger S. Goody and Robert M. Sweet for continuous support and stimulating discussions. We also thank Lisa Wiesmüller for kindly providing an $UmpK_{dicty}$-overproducing *Escherichia coli* strain and Christoph Siethoff for performing the mass spectroscopic analysis of crystals.

REFERENCES

Antonny, B., & Chabre, M. (1992) *J. Biol. Chem. 267,* 6710−6718.
Bell, N. A. (1972) *Adv. Inorg. Chem. Radiochem. 14,* 255 (abstract).
Brune, M., Schumann, R., & Wittinghofer, F. (1985) *Nucleic Acids Res. 13,* 7139−7151.
Brünger, A. T. (1992) in *X-PLOR Version 3.1 - A System for X-ray-Crystallography and NMR*, Yale University Press, New Haven, CT.
Byeon, I. J. L., Shi, Z. T., & Tsai, M.-D. (1995) *Biochemistry 34,* 3172−3182.
Coleman, D. E., Berghuis, A. M., Lee, E., Linder, M. E., Gilman, A. G., & Sprang, S. R. (1994) *Science 265,* 1405−1412.
Dahnke, T., Zhengtao, S., Honggao, Y., Jiang, R.-T., & Tsai, M.-D. (1992) *Biochemistry 31,* 6318−6328.
Feldhaus, P., Fröhlich, T., Goody, R. S., Isakov, M., & Schirmer, R. H. (1975) *Eur. J. Biochem. 57,* 197−204.
Fisher, A. J., Smith, C. A., Thoden, J. B., Smith, R., Sutoh, K., Holden, H. M., & Rayment, I. (1995) *Biochemistry 34,* 8960−8972.
Goodno, C. C. (1982) *Methods Enzymol. 85,* 116−123.
Herschlag, D., & Jencks, W. P. (1990) *Biochemistry 29,* 5172−5179.
Jencks, W. P. (1975) *Adv. Enzymol. Relat. Areas Mol. Biol. 43,* 219−410.
Jones, T. A., Zou, J.-Y., Cowan, S. W., & Kjelgaard, M. (1991) *Acta Crystallogr. A 47,* 110−119.
Kabsch, W. (1993) *J. Appl. Crystallogr. 24,* 795−800.
Knowles, J. R. (1980) *Annu. Rev. Biochem. 49,* 877−919.
Lienhard, G. E., & Secemski, I. I. (1973) *J. Biol. Chem. 248,* 1121−1123.
Lolis, E., & Petsko, G. A. (1990) *Annu. Rev. Biochem. 59,* 597−630.
Maegley, K. A., Admiraal, S. J., & Herschlag, D. (1996) *Proc. Natl. Acad. Sci. U.S.A. 93,* 8160−8166.
Martin, R. B. (1996) *Coord. Chem. Rev. 149,* 23−32.
Otwinowski, Z. (1992) in *An Oscillation Data Processing Suite for Macromolecular Crystallography*, Yale University Press, New Haven, CT.
Reinstein, J., Schlichting, I., & Wittinghofer, A. (1990a) *Biochemistry 29,* 7451−7459.

Reinstein, J., Vetter, I. R., Schlichting, I., Rösch, P., Wittinghofer, A., & Goody, R. S. (1990b) *Biochemistry 29,* 7440−7450.
Saraste, M., Sibbald, P. R., & Wittinghofer, A. (1991) *Trends Biochem. Sci. 15,* 430−434.
Scheffzek, K., Wiesmüller, L., Kliche, W., & Reinstein, J. (1996) *Biochemistry 35,* 9716−9727.
Sondek, J., Lambright, D. G., Noel, J. P., Hamm, H. E., & Sigler, P. B. (1994) *Nature 372,* 276−279.
Theyssen, H., Schuster, H.-P., Packschies, L., Bukau, B., & Reinstein, J. (1996) *J. Mol. Biol. 263,* 657−670.
Warshel, A., & Aqvist, J. (1991) *Annu. Rev. Biophys. Biophys. Chem. 20,* 267−298.
Wiesmüller, L., Scheffzek, K., Kliche, W., Goody, R. S., Wittinghofer, A., & Reinstein, J. (1995) *FEBS Lett. 363,* 22−24.
Xu, Y. W., Morera, S., Janin, J., & Cherfils, J. (1997) *Proc. Natl. Acad. Sci. U.S.A. 94,* 3579−3583.
Yan, H., Dahnke, T., Zhou, B., Nakazawa, A., & Tsai, M.-D. (1990a) *Biochemistry 29,* 10956−10964.
Yan, H., Shi, Z., & Tsai, M.-D. (1990b) *Biochemistry 29,* 6385−6392.

BI970974C